Wind-Forced Cross-Shelf Circulation on the Northern California Shelf*

E. P. DEVER

Center for Coastal Studies, Scripps Institution of Oceanography, La Jolla, California

(Manuscript received 9 June 1995, in final form 10 May 1996)

ABSTRACT

Velocity time series are used to study cross-shelf circulation on the northern California shelf and to examine classical ideas of locally wind-forced cross-shelf circulation. A simple linear two-dimensional model of cross-shelf transport is compared to estimates of cross-shelf transport in the near surface, interior, and near bottom. In winter, when wind forcing is brief and episodic, model transports are highly correlated to the total surface flow and show some skill in predicting subsurface cross-shelf flow. The same model does not work well below the surface in summer when persistent upwelling is observed. This suggests a two-dimensional wind-forced model of cross-shelf circulation may have more applicability to the brief wind events observed in winter than to the persistent wind events observed in summer. The reason for this is unclear. Numerous factors not included in the simple linear wind-forced model such as mesoscale features, upwelling fronts, the interaction of flow with topography, baroclinic pressure gradients, remote forcing, and small-scale wind stress all affect cross-shelf circulation. It is possible some of these are more pronounced on the northern California shelf in summer.

1. Introduction

Understanding the processes that govern cross-shelf circulation on wind-driven shelves remains an issue of interest. The cross-shelf circulation is intimately associated with wind-driven coastal upwelling. This strongly affects water property distributions on wind-driven shelves including the mean and fluctuating heat and salt balances (Dever and Lentz 1994; Lentz 1987a; Rudnick and Davis 1988; Richman and Badan-Dangon 1983; Bryden et al. 1980). Despite its importance, many difficulties remain in modeling cross-shelf velocity quantitatively, difficulties which are especially apparent when compared to success in modeling alongshelf velocities (e.g., Chapman 1987; Zamudio and López 1994).

Many observational studies of cross-shelf velocity have focused on actively upwelling shelves and have revealed a number of common features of mean and subinertial fluctuating velocities (throughout this paper the term mean will refer to averages over records of one to several months and the term subinertial will refer to records that have been filtered to suppress both tidal and inertial oscillations). At midshelf, cross-shelf velocity has a vertical structure consistent with turbulent surface and bottom boundary layers, separated by a possibly stable interior (Badan-Dangon et al. 1986; Kundu and Beardsley 1991). In the surface boundary layer (SBL), cross-shelf velocity is significantly correlated with the alongshelf wind stress (Smith 1981; Winant et al. 1987) in the sense expected from Ekman dynamics, and transport within the SBL agrees quantitatively with estimates of surface Ekman transport (Lentz 1992). Similarly, the structure of near-bottom cross-shelf velocities suggests veering in an Ekman sense forced by alongshelf interior flow (Kundu 1976; Weatherly and Martin 1978; Dickey and Van Leer 1984; Lentz and Trowbridge 1991).

Interior cross-shelf velocities have been more difficult to interpret in light of simple conceptual models. Classical upwelling theory suggests subsurface cross-shelf transports compensate for wind-driven near-surface transport such that the total cross-shelf transport is zero. Observations do show a tendency for this in a mean as well as fluctuating sense (Allen and Kundu 1978). Moreover, Davis and Bogden (1989) find evidence of an alongshelf pressure gradient whose associated interior geostrophic cross-shelf velocity would act to balance surface Ekman transport. However, the mass balance for both mean (Halpern et al. 1977) and fluctuating (Smith 1981) cross-shelf flow is three-dimensional in that the depth-averaged cross-shelf flow departs from zero. Therefore, even sophisticated numerical models that are two-dimensional have difficulty predicting subsurface cross-shelf velocities quantitatively. Chen and Wang (1990) provide an exception to this; however, even their success could not be replicated (Zamudio and López

* Woods Hole Oceanographic Contribution Number 8963.

Corresponding author address: Dr. Edward P. Dever, Center for Coastal Studies - 0209, Scripps Institution of Oceanography, University of California at San Diego, 9500 Gilman Dr., La Jolla, CA 92093-0209.
E-mail: dever@coast.ucsd.edu

1994). Observed cross-shelf velocities also differ in other ways from the classic two-dimensional upwelling model in that interior fluctuations have short correlation scales (Kundu and Allen 1976; Dever 1995) and are more energetic than predicted by linear wind-forced models (Brink et al. 1994). A variety of explanations for this have been suggested including small-scale turbulence (Kundu and Allen 1976) and sensitivity of cross-shelf velocity to small-scale alongshelf wind variability (Brink et al. 1994).

The purpose of this study is to examine velocities on a wind-driven shelf and to use these observations to test the predictions of two-dimensional upwelling theory within the surface boundary layer, interior, and bottom boundary layer. The study includes observations taken on the northern California shelf in winter when alongshelf wind forcing was intermittent and variable in direction as well as summer observations when winds were strong, relatively steady, and generally upwelling favorable.

The remaining structure of this paper is as follows. In section 2 the observations used in the study are introduced. The mean and fluctuating cross-shelf velocities are presented in section 3 in order to gain insight into the response of cross-shelf circulation to wind stress conditions that prevail on the northern California shelf in winter and summer. In section 4, I apply a simple analytical model of wind-forced cross-shelf transport and compare it quantitatively with estimates of cross-shelf transport in the surface, interior, and bottom boundary layers. Results are summarized in section 5.

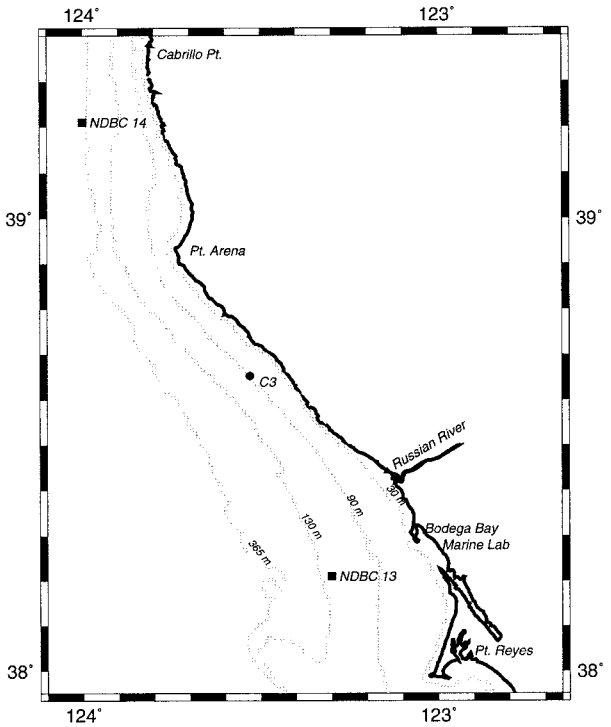

FIG. 1. Map of the northern California shelf showing the nominal location of the central C3 site occupied in 1982 during CODE-2 and in 1988–89 during SMILE and STRESS. Exact locations varied several km between experiments. Total water depth at the CODE-2 C3 site was 90 m, while that at the STRESS C3 site was 97 m. For reference, National Data Buoy Center locations 46013 (NDBC 13) and 46014 (NDBC 14) are also shown.

2. Measurements

The observations used here are from the central C3 locations of the summer 1982 Coastal Ocean Dynamics Experiment (CODE-2) and the winter 1988/89 Shelf Mixed Layer Experiment (SMILE) and Sediment Transport Events on Shelves and Slopes (STRESS) study (Fig. 1).

During CODE-2, C3 was instrumented with a surface mooring including a vector averaging wind recorder (VAWR) and 3 vector measuring current meters (VMCMs) at depths from 5 to 15 m and a subsurface mooring with 8 VMCMs from 10 to 83 m depth. All VMCMs also included temperature sensors. The record examined here extends from 0400 UTC 5 April 1982 to 1800 UTC 25 July 1982. This period begins just prior to the 1982 spring transition to coastal upwelling (Lentz 1987b) and includes the CODE-2 common analysis period (Winant et al. 1987). The CODE observations have been extensively studied (Beardsley and Lentz 1987); two of the most complete descriptions of the CODE-2 moored velocity time series are found in Limeburner (1985) and Winant et al. (1987).

SMILE and STRESS also used surface and subsurface moorings to obtain complete vertical coverage at C3. The C3 SMILE surface mooring included a VAWR and 12 VMCMs at depths from 5.5 to 49.5 m. The STRESS subsurface mooring included 5 vector averaging current meters (VACMs) from 67 to 91 m depth. All of these current meters also measured temperature. Several SMILE VMCM time series ended early due to VMCM bearing failures. The period selected here for study extends from 0400 UTC 6 December 1988 to 2300 UTC 20 February 1989. This includes the most complete vertical coverage achieved in SMILE and coincides with the winter period examined in Dever and Lentz (1994). Further information concerning the SMILE and STRESS field programs is found in Alessi et al. (1991) and Fredericks et al. (1993).

3. Description of cross-shelf velocities

Observations from both 1982 summer and 1988/89 winter are presented for the sake of completeness. However, the summer 1982 observations have been discussed in detail elsewhere (Winant et al. 1987; Lentz and Trowbridge 1991; Lentz 1992), and the emphasis here is on the winter period.

The local isobath direction of 317°T (Winant et al. 1987) will be used to define the alongshelf direction in this study. As noted by Smith (1981), another commonly

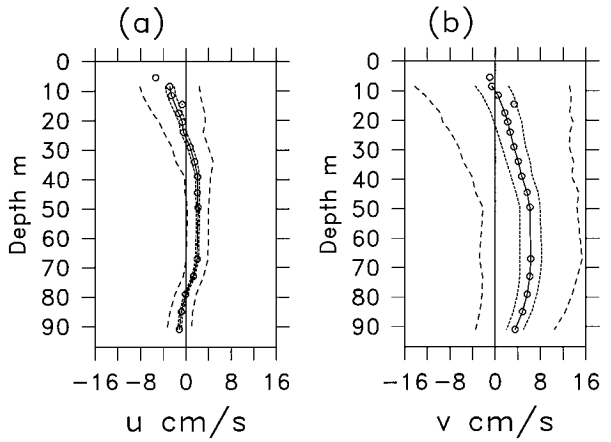

FIG. 2. Mean cross-shelf (a) and alongshelf (b) currents (solid lines) between 0400 UTC 6 December 1988 and 2300 UTC 20 February 1989. Means were calculated from hourly time series. Instrument depths are indicated by open circles. Velocity records that lasted the entire time period are connected; truncated velocity records at 5.5 and 14.5 m are unconnected. Standard deviations (dashed line) and standard errors (dotted line) of low-passed filtered fluctuations of velocity records are also indicated. Standard error estimates are calculated with an integral timescale of 40 h for low-passed cross-shelf velocity fluctuations and 85 h for low-passed alongshelf velocity fluctuations.

TABLE 1. Statistics of mean and low-passed velocity for December 1988–February 1989.

	u (cm s^{-1})				v (cm s^{-1})			
Depth (m)	Mean	Std dev	Correlation to τ_y	Lag h	Mean	Std dev	Correlation to τ_y	Lag h
5.5^{+}	−5.35	6.59	0.50	2	−0.96	17.62	0.41	12
8.5	−2.86	5.25	0.51	1	−0.55	13.68	0.43	13
11.5	−2.55	5.09	0.53	2	0.51	12.95	0.41	15
14.5^{++}	−0.65	3.63	0.73	1	3.40	11.26	0.47	16
17.5	−1.28	4.61	0.47	4	1.73	11.43	0.42	18
20.5	−0.65	4.06	0.36	1	2.22	11.50	0.45	18
24.0	−0.43	3.47	0.26*	2	2.66	10.54	0.47	17
29.0	0.72	3.22	−0.19*	−41	3.30	9.77	0.50	18
34.0	1.51	3.30	0.23*	23	4.09	9.73	0.55	17
39.0	2.06	2.30	−0.15*	0	4.69	8.79	0.56	16
44.5	2.00	2.18	−0.31	0	5.64	9.12	0.58	15
49.5	2.13	1.87	−0.42	2	6.14	8.30	0.58	15
67.0	1.99	1.92	−0.31	−6	6.31	9.06	0.64	14
73.0	1.33	1.78	−0.37	−5	6.16	8.36	0.66	14
79.0	−0.04	1.87	−0.46	0	5.68	7.95	0.68	14
85.0	−0.80	1.99	−0.53	3	4.85	7.53	0.69	13
91.0	−1.16	2.18	−0.62	5	3.53	6.95	0.69	13
$\langle u, v \rangle$	0.20	2.08	−0.17*	−40	4.01	9.00	0.58	15

* Insignificant at 95% level. All record lengths 1844 h except $^{+}$ (811 h) and $^{++}$ (1238 h).

used definition of the alongshelf direction is the principal axis of the depth-averaged velocity. This was roughly 5° clockwise of the local isobath for both summer and winter. Despite this ambiguity in the alongshelf direction, rotation between the local isobath and principal axes coordinates causes little difference for the results presented here; changes of interest will be noted.

The vertical structure of cross-shelf velocities is often interpreted in light of surface and bottom boundary layer theory. The extents of the SBL and BBL are difficult to estimate precisely from measurements. To provide a guide to their thicknesses, the surface and bottom mixed layer thicknesses are estimated here from temperature measurements following Lentz and Trowbridge (1991) and Lentz (1992). The mixed layers do underestimate the entirety of the boundary layers in that a sheared transition layer extends immediately beyond the boundary layers. Possible effects of the surface transition layer will be considered in section 4.

a. Winter cross-shelf velocities

The most basic features of the winter mean cross-shelf velocity profile (Fig. 2, Table 1) are offshore near-surface flow consistent with the mean equatorward wind stress (0.03 N m^{-2}), a vertically uniform flow between 34 and 67 m (extending over both surface and subsurface moorings), and offshore near-bottom flow consistent with the mean interior poleward alongshelf flow. Both the mean alongshelf flow and cross-shelf near-bottom flow oppose the weak mean equatorward wind stress. The mean balance between cross-shelf boundary layer and interior flow is zero to within the uncertainty of the cross-shelf direction. The mean depth-averaged cross-shelf velocity in the 317°T coordinate is 0.20 cm s^{-1} onshore while in the principal axis coordinate it is −0.22 cm s^{-1}.

The mean offshore near-surface and near-bottom velocity depths are qualitatively consistent with the mean surface mixed layer (SML) and bottom mixed layer (BML) thicknesses. The mean SML depth for the winter period is 16.5 m and the mean BML height is 11.1 m above bottom. This suggests that, in a mean sense, the near-surface and near-bottom flows are sampled by several current meters.

Like the mean cross-shelf flow, the subinertial [38 h low-pass filter described in Limeburner (1985)] flow often suggests a wind-forced SBL, an alongshelf velocity-forced BBL, and an interior flow that tends to compensate the boundary layer flows (Fig. 3, Table 1). SBL flow is intermittent in strength, reflecting the nature of winter wind forcing. VMCMs within the top 20 m are generally within the SBL as reflected by their significant correlation with the alongshelf wind stress. Subinertial SBL flow is strongly sheared, and, though the SML appears roughly to describe SBL variability, it can extend below the SML. VMCMs between 24 and 39 m are often below the SBL and correlations with alongshelf wind stress are insignificant here. Interior return flow is generally over a greater range of depths than near-surface flow, weaker in magnitude, and less vertically sheared. Offshore flow in the SBL coupled with interior return flow is common, and is most notable on 24 December, 11 January, and 24 January. Correlations of interior cross-shelf velocity with wind stress, though

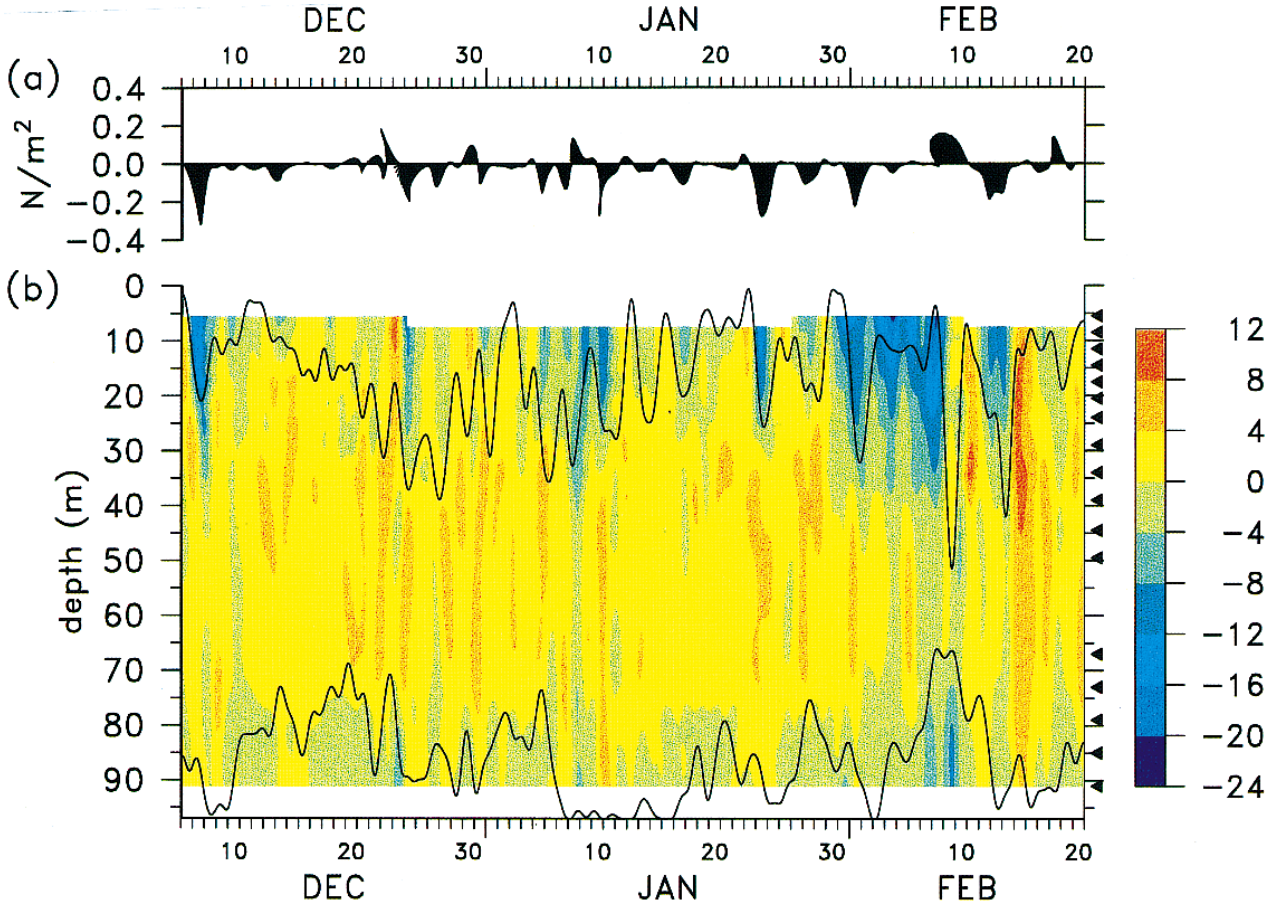

FIG. 3. Low-passed winter 1988/89 wind stress (in dyn cm^{-2}) at C3 (a) and contour plot of subinertial cross-shelf velocities (in cm s^{-1}) (b). Low-passed SML and BML depths are indicated by the solid black lines superimposed on the contour plot. Current meter depths are indicated by black arrows along the right-hand edge.

not as strong as near-surface correlation coefficients, are significant between 44 and 73 m. In this portion of the water column, correlations of cross-shelf velocity with wind stress display the most sensitivity to the choice of coordinate. They increase from −0.3 to −0.4 in the isobath coordinate (317° T) to −0.4 to −0.5 in the principal axis coordinate (323° T). Current meters between 79 to 91 m are often within the BML. At these depths, the correlations between cross-shelf velocity and alongshelf wind stress are still negative but at a positive nonzero lag, in contrast to those near the surface and in the interior. Because near-bottom cross-shelf lags are small compared to alongshelf velocity, they may represent a combination of the interior response (which has near zero lag) and the bottom Ekman response (which should have the same lag as the interior alongshelf velocity). The correlations of alongshelf velocity and near-bottom cross-shelf velocity with alongshelf wind stress imply their variability is dominated by wind forcing, unlike their means.

Though wind forcing is important to cross-shelf velocity, it cannot explain all of its variability. The mean depth-averaged cross-shelf flow is near zero; however, significant depth-averaged cross-shelf velocity fluctuations occur (Fig. 3). The depth-averaged cross-shelf velocity is uncorrelated with the local wind stress, and its standard deviation is roughly equal to that of the total cross-shelf velocity below 34 m (Table 1). Fluctuations in depth-averaged cross-shelf velocity are most notable in late January and in February when it is large relative even to near-surface velocities. Dever and Lentz (1994) also found three-dimensional fluctuations in the heat balance during this period. Because these fluctuations were uncorrelated with local wind forcing and had longer timescales than it, they may be associated with unresolved mesoscale features.

b. Summer cross-shelf velocities

The summer 1982 cross-shelf velocities (Figs. 4 and 5; Table 2) are similar to the winter cross-shelf velocities in some ways, but also display important differences. As in winter, a wind-forced SBL is evident in the mean and fluctuating velocities. This SBL can extend below

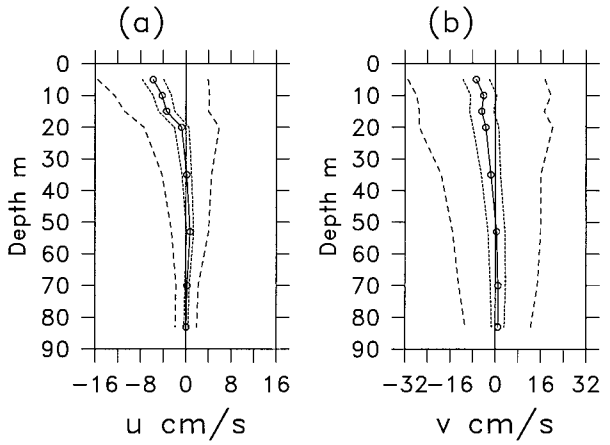

FIG. 4. Mean cross-shelf (a) and alongshelf (b) currents (solid lines) between 0400 UTC 5 April 1982 and 1800 UTC 25 July 1982. Means were calculated from hourly time series. Instrument depths are indicated by open circles. Standard deviations (dashed line) and standard errors (dotted line) of low-passed filtered fluctuations of velocity records are also indicated. Standard error estimates are calculated with an integral timescale of 100 h for low-passed cross-shelf and alongshelf velocity fluctuations.

TABLE 2. Statistics of mean and low-passed velocity for April–July 1982.

	u (cm s^{-1})				v (cm s^{-1})			
Depth (m)	Mean	Std dev	Correlation to τ_y	Lag h	Mean	Std dev	Correlation to τ_y	Lag h
5	−5.78	9.72	0.74	0	−6.68	24.25	0.78	11
10	−4.17	8.38	0.69	−3	−4.07	23.75	0.73	12
15	−3.39	7.40	0.69	0	−4.77	22.07	0.74	12
20	−0.73	6.63	0.55	1	−3.26	23.57	0.74	12
35	0.18	4.37	0.39*	100	−1.47	17.58	0.69	12
53	0.74	3.27	0.31*	16	0.48	15.57	0.67	12
70	0.21	1.96	0.35*	100	0.98	13.88	0.66	12
83	0.02	1.89	−0.35*	7	0.93	11.59	0.70	12
$\langle u, v \rangle$	−0.77	3.44	0.53	2	−1.29	16.88	0.73	12

* Insignificant at 95% level. All record lengths 2679 h. Values differ somewhat from those given in Winant et al. (1987) due to differing start times.

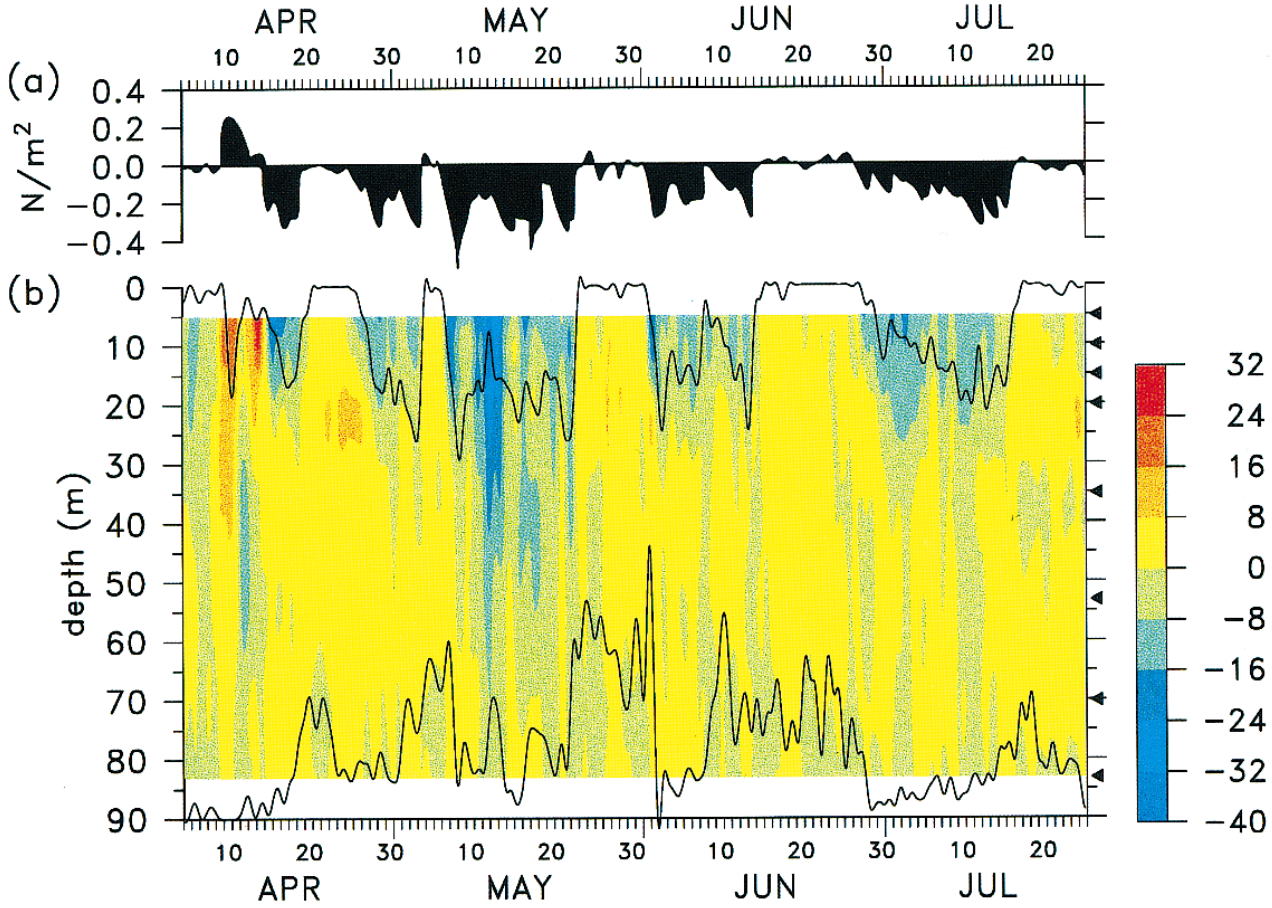

FIG. 5. Low-passed summer 1982 wind stress (in dyn cm^{-2}) at C3 (a) and contour plot of subinertial cross-shelf velocities (in cm s^{-1}) (b). Low-passed SML and BML depths are indicated by the solid black lines superimposed on the contour plot. CODE-2 also included surface and bottom temperature records in addition to current meters (black arrows). Note that the scale ranges differ from Fig. 3.

the SML (Lentz 1992). In contrast to winter, there is little evidence for a return flow beneath the SBL. The summer mean subsurface cross-shelf flow is near zero so that the mean depth-averaged flow is offshore in the local isobath and the principal axes coordinates (reduced to -0.60 cm s^{-1} in the principal axes coordinates). Likewise, subsurface cross-shelf velocities in the local isobath coordinate are not significantly correlated with alongshelf wind stress, though in the principal axes coordinate 70 and 83 m velocities are negatively correlated with alongshelf wind stress (-0.53 and -0.62 respectively with lags of 9 h). The depth-averaged cross-shelf velocity is correlated with the alongshelf wind stress. This correlation is due partly to the offshelf flow during the May upwelling event and to a lesser extent that in July. Magnitudes of cross-shelf velocity fluctuations are greater than those in winter, especially in the SBL and for depth-averaged flow.

4. Interpreting the cross-shelf circulation in terms of vertically integrated transports

Results of section 3 suggest the importance of local wind-forcing to cross-shelf velocity throughout the water column in winter. During this time, the responses of the mean and fluctuating cross-shelf velocities to wind forcing appear similar to those predicted by classical two-dimensional upwelling theory. In contrast, summer observations show local wind forcing is important near the surface but show little evidence below the surface for a simple two-dimensional response to wind forcing. The winter observations suggest that we may be able to apply a relatively simple wind-forced model to cross-shelf velocity with some success. There is reason to expect a simple model to fail in summer. However, a comparison between winter and summer results should highlight the conditions under which a two-dimensional model has some applicability as well as demonstrate the limits of such a model.

a. Application of a two-dimensional cross-shelf transport model

The analytic two-dimensional model adopted here follows directly from the transport models developed in Csanady (1982) and, except for the parameterization of bottom friction, is a transport analog of the velocity model examined by Janowitz and Pietrafesa (1980). The development here is very similar to that in Janowitz and Pietrafesa (1980) but is included in the interest of completeness. Despite its simplicity, the model can simulate the response of distinct surface boundary, interior, and bottom boundary layers to wind forcing and an alongshelf pressure gradient. It includes a large number of simplifying assumptions, the most important of which is two-dimensional volume conservation. Other assumptions include: a rigid lid, an implicit three-layer structure of flow (distinct and separate boundary layers), no dynamical role for density gradients, linear dynamics including linear bottom friction, and boundary layers that are at steady state with surface and bottom stresses. For a right-handed coordinate system where x and y are the cross-shelf and alongshelf directions and $x = 0$ at the coast, the vertically integrated alongshelf momentum equation under these assumptions is

$$\frac{\partial V}{\partial t} + fU = -gh\zeta_y + \frac{\tau_s^y}{\rho} - \frac{\tau_b^y}{\rho}. \tag{1}$$

Here U and V are the vertically integrated cross-shelf and alongshelf transports, f is the Coriolis parameter, $gh\zeta_y$ is the shallow water alongshelf pressure gradient assuming no density contribution, τ_s^y is the alongshelf wind stress, τ_b^y is the alongshelf bottom stress, and ρ is a constant density set equal to 1026 kg m^{-3}.

The coastal boundary condition of $U = 0$ and the vertically integrated two-dimensional continuity equation imply $U = 0$ for all x. To solve (1), U is divided into surface, interior, and bottom boundary components; that is,

$$0 = U = U_{\mathrm{SE}} + U_{\mathrm{I}} + U_{\mathrm{BE}}, \tag{2}$$

where, for timescales long compared to f, the cross-shelf surface Ekman solution is $U_{\mathrm{SE}} = \tau_s^y/\rho f$ and the cross-shelf bottom Ekman solution is $U_{\mathrm{BE}} = -\tau_b^y/\rho f$. Here U_{SE} is estimated from measured wind velocity using the Large and Pond (1981) neutral stability bulk formula, and U_{BE} is estimated from a linear drag law using modeled interior velocities. Because direct estimates of bottom stress acquired as part of STRESS are approximately 45° from the interior flow direction, τ_b is here estimated by solving for a bottom Ekman layer rather than using a linear drag law, which assumes bottom stress is in the direction of interior velocity. The bottom Ekman layer equations with a constant eddy viscosity A, and boundary conditions far from the bottom given by interior velocity components u_I and v_I lead to (e.g., see, Pedlosky 1979)

$$\tau_b^y = \frac{\rho A}{\delta}(u_I + v_I) = \frac{\rho \delta f}{2}(u_I + v_I), \tag{3}$$

where $\delta = (2A/f)^{0.5}$ is the bottom Ekman layer thickness. Assuming interior velocities are constant with respect to depth, $u_I = U_I/h$ and $v_I = V_I/h$, where h is the total water depth, the bottom Ekman transport is

$$U_{\mathrm{BE}} = -\frac{\tau_b^y}{\rho f} = -\frac{\delta}{2h}(U_I + V_I). \tag{4}$$

Equation (4) is consistent with the tensor formulation (Jenter and Madsen 1989) of bottom stress for a constant eddy viscosity model. It differs from the common linear drag law, which would lead to $\tau_b^y = \tau V_I/h$ but because $V_I \gg U_I$, the choice of (4) or the traditional linear drag law has little effect on τ_b^y.

Assuming an inviscid interior, the interior transports are governed by

$$\frac{\partial V_I}{\partial t} + fU_I = -gh\zeta_y. \tag{5}$$

Together (2), (4), and (5) form a set of coupled first-order linear ordinary differential equations for U_I, $U_{\rm BE}$, and V_I. Equations (4) and (5) contain two unknown variables, ζ_y and δ. No systematic attempt was made to choose these variables in a best fit sense, rather physically reasonable values were chosen a priori.

A mean ζ_y is chosen as a mechanism to account for the tendency for poleward alongshelf flow in the absence of a strong equatorward wind stress. Based on observed mean alongshelf flows, this value is set at -5×10^{-8} in winter and -1.2×10^{-7} in summer. These values agree in magnitude with the alongshelf gradients found for the northern California shelf by Hickey and Pola (1983), though the winter ζ_y must be of the opposite sign in order to account for the observed poleward flow. The alongshelf pressure gradient affects only the mean transports; all variability in the model is locally wind forced. It would be possible to include fluctuating pressure gradients resulting from coastal-trapped waves as Zamudio and López (1994) do; however, they found the cross-shelf velocity response to remote pressure gradients was secondary to that of local wind forcing, and the emphasis here is on identifying and interpreting the response of cross-shelf flow to local wind forcing.

The parameter δ sets the strength of the bottom friction. It is taken as 6 m based on bottom acoustic shear sensor (BASS) estimates of bottom shear velocity during STRESS and CODE-2 (Gross et al. 1992; Grant et al. 1984). This friction parameter corresponds to a linear drag coefficient of about 3×10^{-4}m s^{-1} or a quadratic drag coefficient of about 3×10^{-3}. It yields bottom shear velocities of 0.5–1.0 cm s^{-1}, in agreement with typical BASS estimates.

Given ζ_y and δ, a solution to (2), (4), and (5) can be found easily by using (4) to solve for U_I in (2):

$$U_I = \frac{-U_{\rm SE} + \epsilon V_I}{1 - \epsilon}, \tag{6}$$

where $\epsilon = \delta/2h$. Equation (6) in turn can be substituted into (5) to give a first-order differential equation in terms of V_I:

$$\frac{\partial V_I}{\partial t} + \beta V_I = \frac{\beta U_{\rm SE}}{\epsilon} - gh\zeta_y = F(t), \tag{7}$$

where β is $\epsilon f/(1 - \epsilon)$. The solution to (7) is

$$V_I = e^{-\beta t}\left[\int_0^t e^{\beta t'} F(t')\, dt' + C\right]. \tag{8}$$

The constant of integration, C, is given by the interior transport specified at $t = 0$.

As a simple example of the behavior of (8), assume $\zeta_y = 0$, $\tau_s^y = $ const, and $V_I = 0$ at $t = 0$. Then the solution to (8) is

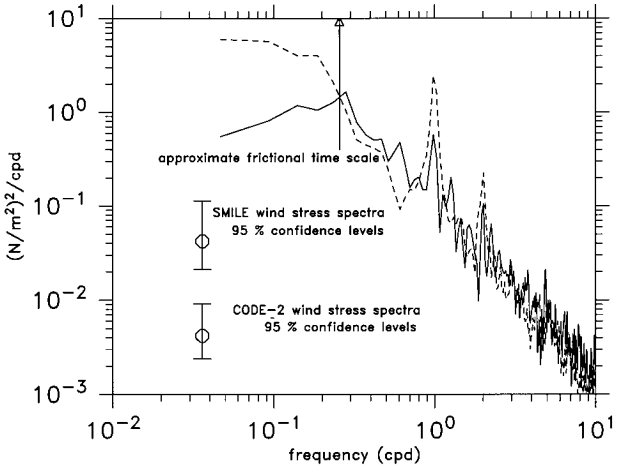

FIG. 6. Alongshelf wind stress spectra. SMILE (solid) and CODE-2 (dashed) spectra show similar variability for periods between 1 and 4 days. The CODE-2 wind spectrum is affected by persistent upwelling favorable winds, which last up to three weeks, and shorter relaxation events, which can last a week or more; hence it shows more variability for periods longer than 4 days (longer than SMILE).

$$V_I = \frac{1}{\epsilon} U_{\rm SE}(1 - e^{-\beta t}), \tag{9}$$

with U_I and $U_{\rm BE}$ given by (6) and (2) for this set of forcing conditions as

$$U_I = -U_{\rm SE}\frac{e^{-\beta t}}{1 - \epsilon} \tag{10}$$

and

$$U_{\rm BE} = U_{\rm SE}\left(\frac{e^{-\beta t}}{1 - \epsilon} - 1\right). \tag{11}$$

The factor $1/\beta$ gives the frictional timescale of the model. For $\delta = 6$ m, $1/\beta$ is about 4 days at the C3 location. The subsurface cross-shelf transport for times short compared to $1/\beta$ is primarily in the interior rather than BBL. For times longer than $1/\beta$, $U_{\rm BE}$ becomes larger than U_I and at steady state, the subsurface cross-shelf transport is entirely in the BBL.

The frictional timescale, $1/\beta$, indicates seasonal differences in wind stress on the northern California shelf cause seasonal differences in the model response. In winter, the dominant timescales of wind forcing are generally three days or less; hence the subsurface winter model response is primarily in the interior. In summer, persistent upwelling favorable winds lasting several weeks are common and lead to a subsurface model response primarily in the BBL. This seasonal difference is indicated by spectra of alongshelf wind stress (Fig. 6), which show variability at frequencies lower than $1/\beta$ is greater in the summer of 1982 than in the winter of 1988/89.

In practice, the model is forced with the 38-h low-passed τ_s^y. Equation (8) is integrated numerically to get

V_I. Beyond the frictional timescale (4 days), the model is insensitive to the initial condition; here the initial condition is the observed V at $t = 0$. Then U_I and U_{BE} are determined from (2) and (6).

The total flow within the SBL is U_{SE} plus that portion of U_I within the SBL. The interior transport is assumed to be uniform with depth so that the total model surface transport is

$$U_S = U_{SE} + \frac{\delta_S U_I}{h}, \tag{12}$$

where δ_S is an estimate of the SBL depth and h is the total depth (90 m for CODE-2 and 97 m for SMILE and STRESS). The modeled U_I and U_B are similarly represented as

$$U_I' = U_I\left(1 - \frac{\delta_S + \delta_B}{h}\right) \tag{13}$$

and

$$U_B = U_{BE} + \frac{\delta_B U_I}{h}. \tag{14}$$

The total alongshelf transport, V, was also calculated from $V = V_{SE} + V_I + V_{BE}$, where V_{SE} and V_{BE} were estimated from the cross-shelf wind stress and the analog of (4), respectively.

In (12), (13), and (14), δ_S and δ_B represent observational estimates of the SBL and BBL thicknesses. Figures 3 and 5 and earlier work (e.g., Lentz 1992) indicate the SML depth provides a minimum bound on the SBL, but that the SBL includes some transition region below the SML. The exact depth of the transition region is difficult to estimate from observations. Lentz (1992) explored several ways to include it. He compared Ekman layer transports with observed SML transports and with transports in a SBL that included the SML and a transition layer scaled as 50% of the SML. Modeled and observed transports will here be considered in the same way to gauge effects of a surface transition layer. The extent of the BBL is even more elusive. Trowbridge and Lentz (1991) and Lentz and Trowbridge (1991) formulated and applied a bottom mixed layer model to several upwelling shelves with encouraging results, but to date there have been few observations capable of verifying a bottom boundary transition layer. In the absence of any better information, the BML will be used as an estimate of the BBL extent.

Modeled transports are compared with observed transports estimated by trapezoidal integration of velocities within the SML, SML plus a transition layer (SM+TL), interior, and BML. As in Dever and Lentz (1994), uniform extrapolation is used above and below the shallowest and deepest current meters and linear interpolation is used to bridge any gaps in interior current meter records. Examination of cross-shelf transport within dynamic regions simplifies interpretation of current meter records, which are at fixed depths whereas dynamical flow regions vary in depth. This approach has been used before (Badan-Dangon et al. 1986); however, the vertical resolution of CODE-2, SMILE, and STRESS make possible the use of empirical estimates of boundary and interior layer thicknesses throughout the water column rather than the indirect subsurface theoretical scales utilized by Badan-Dangon et al. (1986).

Both the CODE-2 and SMILE and STRESS velocity records resolve near-surface and interior flow. However, it is possible that the reduced (relative to SMILE and STRESS) vertical resolution of the CODE-2 C3 mooring affects transport estimates in the BML, which was usually sampled by only one current meter (Lentz and Trowbridge 1991).

b. Comparison of observed and modeled cross-shelf transports for winter 1988/89

Modeled cross-shelf transports are compared to total (Fig. 7 and Table 3) and depth-dependent (Fig. 8 and Table 3) transports. The depth-dependent transports are calculated by subtracting the depth-averaged cross-shelf velocity from the total cross-shelf velocity. This is done to focus the model comparison to the depth structure of the observed flow, which the model is capable of representing, rather than the depth-averaged cross-shelf flow, which the model is incapable of representing. Comparisons of modeled to depth-dependent transports should be viewed with caution. If, for example, the SML (or SM+TL) transport is highly correlated with local wind forcing, but the interior and BML transport are uncorrelated with local wind forcing, removal of the depth-averaged cross-shelf velocity results in an increased correlation of interior and BML transport with wind stress. This would be accompanied by a decreased correlation coefficient of near-surface transport with wind stress and a decrease in the regression coefficient of depth-dependent near-surface transport with modeled near-surface transport. This is not the case in winter as the correlation of depth-dependent near-surface transport with the wind-forced model is actually higher, and little change in the regression coefficient occurs.

Modeled and estimated near-surface cross-shelf transports agree most closely. Both the total (Fig. 7) and depth-dependent (Fig. 8) near-surface transports are well correlated with regression coefficients near 1 (Table 3). Estimated near-surface transport is relatively insensitive to removal of the depth-averaged transport. Its most noticeable effect is an improvement in model and estimate agreement in February (Figs. 7 and 8). Addition of a transition layer equal to 50% of the SML depth does not noticeably improve agreement between the model and the observations relative to the SML case (Table 3). Though the regression coefficient increases slightly to greater than one, this is accompanied by a decrease in the near-surface correlation.

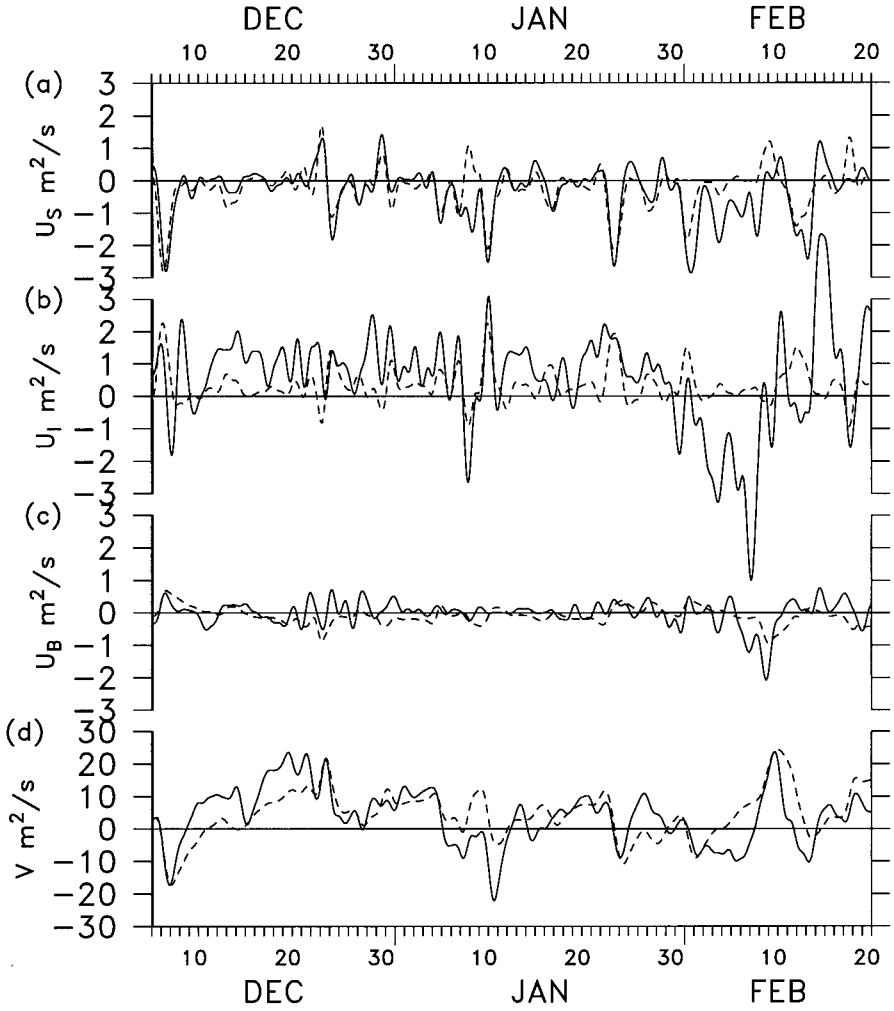

FIG. 7. Modeled and total (including depth-averaged) estimated transports for winter 1988/89. (a) Cross-shelf SML transport (solid) with modeled transport (dashed) in the SML. Modeled and estimated transports within the SML+TL are qualitatively very similar to SML transports. (b) Cross-shelf interior (below the SML) transport and modeled transport in the interior. Exclusion of a transition layer does not improve agreement between observed and modeled interior transports. (c) Cross-shelf BML transport with modeled transport in the BML. (d) Alongshelf transport and modeled alongshelf transport.

TABLE 3. Statistics of model comparison to total and depth-dependent transports estimated from observations for December 1988–February 1989. The number of independent observations is estimated by the record length (1844 h) divided by the integral timescales. Based on observations, these are assumed to be 40 h for U transports and 85 h for V transports. For this integral timescale, correlation coefficients of .29 (.43) or higher are significant at the 95% level for U (V) transports; 0 lagged (r_0) correlation coefficients are presented. The slope of the regression line (a) (Draper and Smith 1966) where (OBS − $\overline{\text{OBS}}$ = a(MOD − $\overline{\text{MOD}}$) is also indicated.

	Means (m^2 s^{-1})			σ (m^2 s^{-1})			r_0		a	
	Model	Total	Depth-dependent	Model	Total	Depth-dependent	Total	Depth-dependent	Total	Depth-dependent
U_{SML}	−0.25	−0.34	−0.34	0.63	0.78	0.62	.70	.85	0.87	0.84
U_I	0.33	0.54	0.36	0.51	1.47	0.52	.21	.73	0.60	0.74
$U_{\text{SM+TL}}$	−0.19	−0.34	−0.34	0.54	1.01	0.60	.58	.82	1.07	0.91
$U_{I-\text{TL}}$	0.28	0.55	0.36	0.43	1.27	0.52	.27	.70	0.80	0.85
U_{BML}	−0.09	−0.01	−0.02	0.26	0.37	0.34	.39	.43	0.57	0.57
V	4.39	3.89		7.40	8.73		.61		0.72	

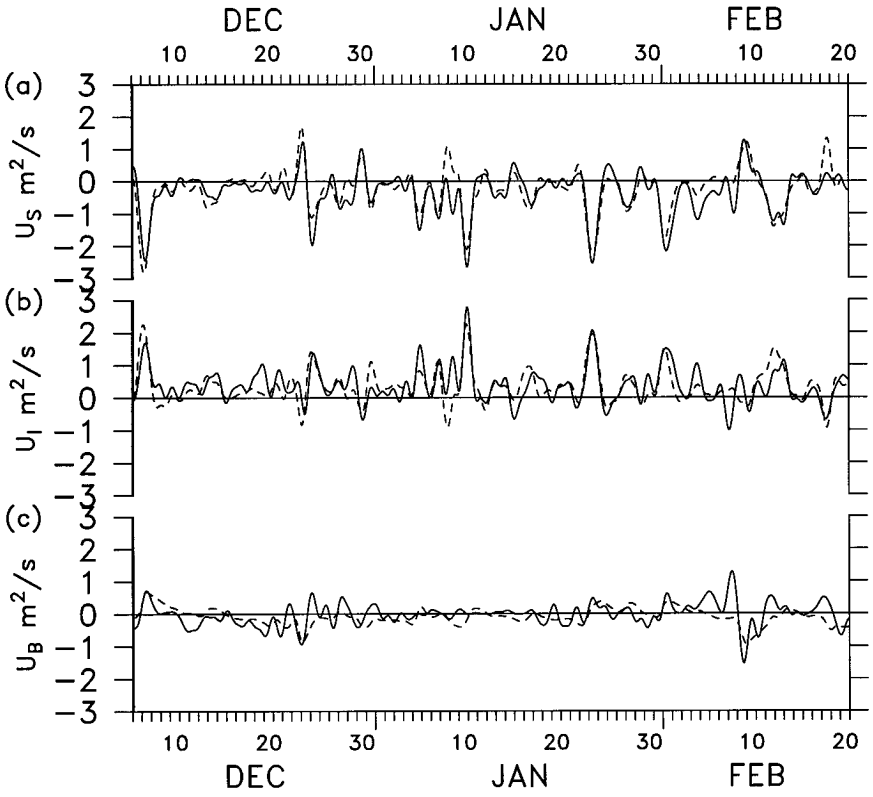

FIG. 8. Modeled and depth-dependent estimated transports for winter 1988/89. (a) Cross-shelf SML transport (solid) with modeled transport (dashed) in the SML. Modeled and estimated transports within the SML+TL are qualitatively very similar to SML transports. (b) Cross-shelf interior (below the SML) transport with modeled transport in the interior. Exclusion of a transition layer does not improve agreement between observed and modeled interior transports. (c) Cross-shelf BML transport with modeled transport in the BML.

Comparison of modeled and total cross-shelf transport is poorest within the interior (Fig. 7 and Table 3). Correlation between observed and modeled interior transport is not significant at the 95% level in the 317°T reference frame. It is reduced mostly by the strong depth-averaged cross-shelf transport in February. Rotation to 323°T improves correlation to total interior transport slightly. If attention is focused on the time period between 0400 6 December 1988 and 2300 31 January 1989 when U is generally weak, then correlation coefficients between the wind-forced model and total interior transport increase, as is qualitatively indicated in Fig. 7. This result is again particularly apparent in the 323°T reference frame. Onshore interior return flow associated with several upwelling events is most notable on 8 December, 11 January, and 24 January. The transition layer case (Table 3) results in a slight improvement in observation and model correlation and regression; however, the correlation between total interior cross-shelf flow and modeled interior cross-shelf flow remains insignificant at the 95% level.

Modeled and estimated cross-shelf transports within the BML agree fairly well. Agreement is not improved by removing the depth-averaged cross-shelf flow. Both interior and bottom Ekman flow are important to the modeled near-bottom cross-shelf transport (14). Even if bottom friction were modeled perfectly, the bottom Ekman transport would only be determined accurately to the extent to which the locally wind-forced transport model describes alongshelf transport.

Comparison of the modeled and estimated alongshelf transport shows a high correlation and a regression coefficient near one. Since the modeled alongshelf transport is dominated by the interior alongshelf transport, V_I, and fluctuations in V_I are determined entirely by interior cross-shelf transport (5), the high correlation between modeled and observed alongshelf transport is taken as further evidence of the applicability of the locally forced two-dimensional model in winter. It is possible to abandon any attempt to calculate alongshelf transport and instead use the observed alongshelf transport to model the bottom Ekman transport. However, this does not substantially improve agreement between the estimated and modeled bottom Ekman transport in winter, and the insight on the role of the interior cross-shelf transport in (5) is lost.

TABLE 4. Statistics of model comparison to transports estimated from observations for April 1982–July 1982. The number of independent observations is estimated by the record length (2679 h) divided by the integral timescales. Based on observations, these are assumed to be 100 h for U and V transports. For this integral timescale, correlation coefficients of .38 or higher are significant at the 95% level; 0 lagged (r_0) correlation coefficients are presented. The slope of the regression line (a) where (OBS − $\overline{\text{OBS}}$ = a(MOD − $\overline{\text{MOD}}$) is also indicated.

	Means ($m^2\ s^{-1}$)			σ ($m^2\ s^{-1}$)			r_0		a	
	Model	Total	Depth-dependent	Model	Total	Depth-dependent	Total	Depth-dependent	Total	Depth-dependent
U_{SML}	−1.05	−0.75	−0.54	1.18	1.02	0.70	.84	.86	0.73	0.51
U_I	0.84	−0.01	0.42	0.76	2.21	0.54	−.16	.40	−0.46	0.28
U_{SM+TL}	−0.96	−1.00	−0.41	1.08	1.42	0.59	.81	.75	1.07	0.41
U_{I-TL}	0.75	0.23	0.29	0.68	1.91	0.50	−.09	.30	−0.26	0.22
U_{BML}	0.21	0.07	0.13	0.91	0.37	0.41	−.07	.47	−0.03	0.21
V	−2.58	−1.16		24.76	15.19		.49		0.30	

c. *Comparison of observed and modeled cross-shelf transports for summer 1982*

Comparison of modeled and estimated cross-shelf transports during CODE-2 (Table 4, and Figs. 9 and 10) shows the local wind forcing, linear dynamics, and two-dimensional continuity incorporated in the model cannot account for observed cross-shelf circulation below the surface. The near-surface model response is dominated by the surface Ekman transport, which is well correlated with observations (Lentz 1992). Addition of a transition layer equal to 50% of the SML depth improves agreement between the model and the observations relative to the SML case (Table 4) in that the regression coefficient increased with little decline in the correlation. Modeled interior and bottom transports are uncorrelated with total observed interior and bottom transports, and the modeled interior variability is much less than that of the total observed interior transport (Fig. 9). Exclusion of a surface transition layer from the interior transport does not improve agreement between observed and modeled interior transport. Observed variability in the interior transport is due largely to depth-averaged cross-shelf flow, which as indicated by its standard deviation (Table 2) is greater than that observed in winter (Table 1). Even when the model is compared to the depth-dependent transport (Fig. 10), correlation coefficients between observed and modeled subsurface transports remain lower than in winter. Moreover, the regression coefficient between the observed and modeled near-surface transport is reduced. The most noticeable improvement in agreement between modeled transports and estimated depth-dependent transports occurs in the BML, which follows the predicted model behavior for long timescales. Much of the disagreement between the modeled BML transport and observed depth-dependent BML transport in summer is explained by the imperfect ability of the model to predict interior alongshelf transport. When the observed rather than modeled alongshelf transport is used to force the bottom Ekman layer transport, the modeled and observed depth-dependent bottom transports agree much more closely. For this case, the zero lag correlation is 0.75 with a regression coefficient of 0.64 compared to a correlation of 0.47 and regression coefficient of 0.21 in Table 4.

Some of the inability of the transport model to explain subsurface cross-shelf circulation in summer may be accounted for by inclusion of variable alongshelf pressure gradients in (5). Such gradients may be caused by remote (CTW) processes (López and Clarke 1989) or associated with local wind relaxation events (Brown et al. 1987). Addition of alongshelf pressure gradients estimated from observations to (5) slightly improves model agreement with depth-dependent quantities, but does nothing to improve agreement with total observed subsurface transport. Baroclinic pressure gradients could also affect subsurface cross-shelf transport; however, the relative lack of success of a model incorporating both baroclinic and CTW pressure gradients (Zamudio and López 1994) and the large variability in depth-averaged cross-shelf transport demonstrate the importance of three-dimensional processes.

It is uncertain why three-dimensional processes may have greater importance in summer. Three possible reasons include offshore mesoscale variability, a nonlinear response to persistent wind forcing, and a complicated ocean response to wind relaxation events. In 1987, Kosro et al. (1991) found mesoscale variability in a region extending from 60 to 150 km off the northern California coast to be greater in two cruises that occurred after the transition to strong upwelling rather than during two similar cruises in winter. Some of this variability may affect shelf circulation. For example, Lentz (1987a) described a shallow lens of warm water that extended from over 35 km offshore onto the shelf during CODE-2. This lens strongly affected shelf circulation from 27 June through 7 July 1982, a period which included wind-driven offshore flow near the surface (see Figs. 5, 9, and 10). In addition to offshore variability, it is likely that the local response to strong persistent wind forcing causes a breakdown in two-dimensional models of wind-driven circulation. In a numerical model, Chen (1990) found nonlinear and vertical shear stress terms in the interior alongshelf momentum balance became larger after 5 days of steady wind forcing. In reality,

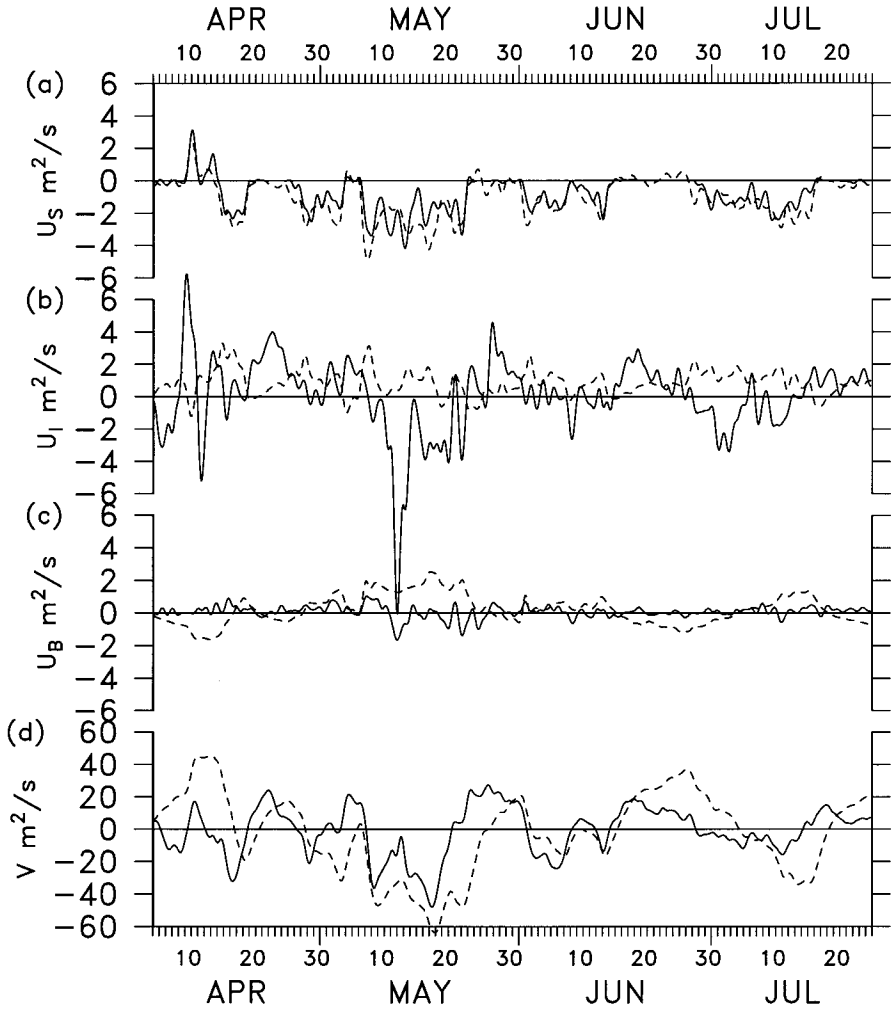

FIG. 9. Modeled and total (including depth-averaged) estimated transports for summer 1982. Note the *y*-axis scales have been expanded by a factor of 2 relative to Figs. 7 and 8. (a) Cross-shelf SML transport (solid) with modeled transport (dashed) in the SML. Modeled and estimated transports within the SML+TL are qualitatively similar to SML transports, though estimated transport magnitudes are slightly larger. (b) Cross-shelf interior (below the SML) transport with modeled transport in the interior. Exclusion of a transition layer does not improve agreement between observed and modeled interior transports. (c) Cross-shelf BML transport with modeled transport in the BML. (d) Alongshelf transport and modeled alongshelf transport.

strong wind-forcing for a period of 5 days could cause development of an upwelling front (de Szoeke and Richman 1984). Instability along an upwelling front could lead to short wavelength (approximately 20 km) features on timescales of days (Barth 1994). This would likely cause a breakdown in any two-dimensional response of interior cross-shelf velocity to persistent summer wind forcing. Finally, the ocean response to wind relaxation events on the northern California shelf is quite complicated. Send et al. (1987) found onshore flow associated with wind relaxation events occurs over the outer shelf as turbulent motions with scales less than 25 km rather than as onshore displacement of an upwelling front. However, even if wind relaxation events are excluded, the transport model still performs poorly below the SBL in summer.

5. Summary

Velocity time series have been used to study the cross-shelf circulation on the northern California shelf. The focus has been on the cross-shelf velocity response to the contrasting types of wind forcing that prevail in the winter and the summer. In winter, along-shelf wind stress variability is concentrated at periods of 2–3 days, and both poleward and equatorward fluctuations occur. In summer, significant wind stress variability occurs for longer durations. Equatorward wind events lasting two

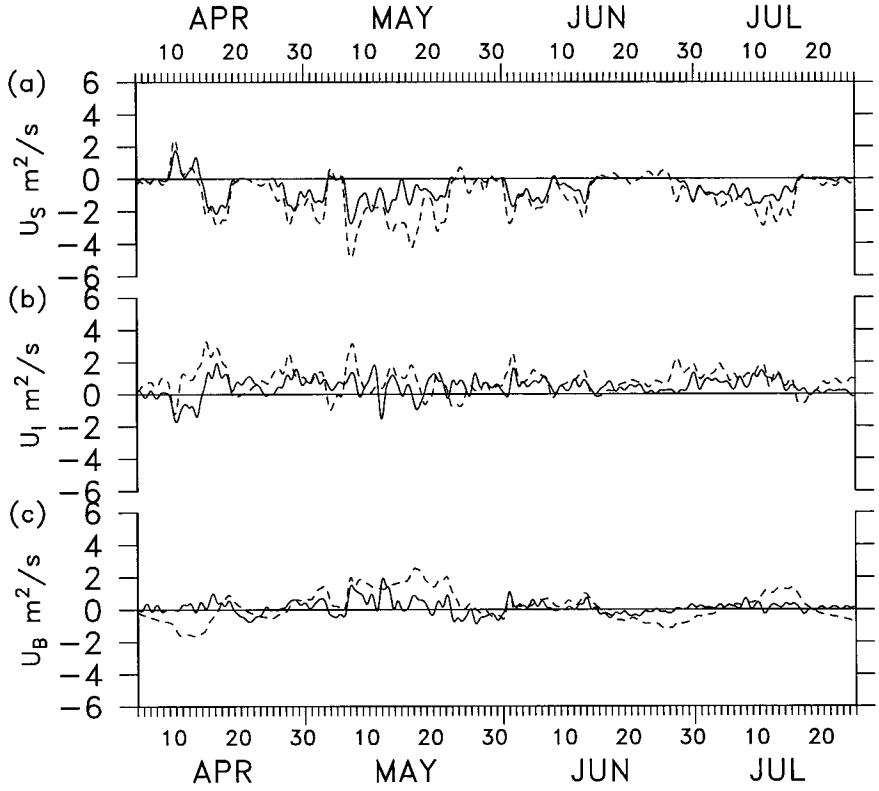

FIG. 10. Modeled and depth-dependent estimated transports for summer 1982. Note the *y*-axis scales have been expanded by a factor of 2 relative to Figs. 7 and 8. (a) Cross-shelf SML transport (solid) with modeled transport (dashed) in the SML. (b) Cross-shelf interior (below the SML) transport with modeled transport in the interior. Exclusion of a surface transition layer does not improve agreement between observed and modeled interior transports. (c) Cross-shelf BML transport with modeled transport in the BML.

to three weeks are common. These are separated by weak (occasionally poleward) winds lasting about one week.

A descriptive view of the cross-shelf circulation between December 1988 and February 1989 suggests its response to winter wind forcing is often similar to that predicted by two-dimensional upwelling theory. However, between April and July 1982 the cross-shelf circulation indicates a more complicated response to wind forcing. Though the summer near-surface cross-shelf velocity resembles that predicted by Ekman theory, there is little evidence in the interior or near-bottom cross-shelf velocities for a two-dimensional response to wind forcing.

To test theoretical predictions in a more quantitative way, a simple model of wind-forced transport was applied to both winter and summer observations. Model assumptions included two-dimensionality, linear dynamics, and purely barotropic pressure gradients. Model predictions were compared with observed transports integrated through empirical estimates of the surface boundary, interior, and bottom boundary layers. Two estimates of the surface boundary layer depth were considered. A surface mixed layer (SML) depth was estimated from temperature observations, and a deeper boundary layer was considered by including a transition region below the SML equal to 50% of the SML depth. The bottom boundary layer thickness was estimated from the bottom mixed layer (BML) height, and the interior extended from the bottom of the surface boundary layer estimate to the top of the BML.

Despite the model's strict assumptions, it was capable of simulating much of the cross-shelf transport in winter. The modeled near-surface transport was dominated by the surface Ekman transport and highly correlated with the observations. Inclusion of a surface transition layer did not strongly affect results. Below the surface, the model showed some skill in predicting interior and bottom cross-shelf transports during the first two-thirds of the winter study period and did surprisingly well in describing the depth-dependent cross-shelf transport over the entire period. For the relatively short timescales of wind forcing in winter, the model predicted, and the data seemed to indicate, a subsurface response primarily in the interior rather than in the bottom boundary layer.

In comparison to winter, the wind-forced model did not work well in summer. Though modeled and estimated near-surface transports agreed well, modeled and

estimated interior and BML transports did not. Inclusion of a surface transition layer improved agreement between modeled and estimated near-surface transport magnitudes, but did not improve interior cross-shelf transport comparisons. Some of the model's failure can be explained by its neglect of nonlinear processes, baroclinic pressure gradients, and remote forcing; however, most can probably be attributed to its assumption of two-dimensionality.

The simple wind-forced transport model is limited by the physical processes and dynamics it considers. Numerous other factors that can influence cross-shelf velocity include: mesoscale eddies, upwelling fronts, variable topography, and small-scale wind stress. Dynamical processes that may be important include: nonlinear dynamics, interior shear stress, and baroclinic pressure gradients. All of these can make the cross-shelf flow strongly three-dimensional. The success of the two-dimensional transport model in winter relative to summer suggests some of these factors become more important under the steadier wind-forcing conditions prevalent on the northern California shelf in summer. A careful numerical modeling effort may be able to determine the circumstances under which quasi-two-dimensional dynamics apply to cross-shelf velocity and study the question of seasonal variability in cross-shelf dynamics on wind-forced shelves.

Acknowledgments. Financial support was provided by NSF Grant OCE 91-15713. This work was done as part of my thesis in the MIT/WHOI Joint Program in Oceanography, and I thank my advisor, Steve Lentz, for guidance and feedback through all its stages. I also thank my committee members: Jim Price, Ken Brink, Bob Beardsley, Paola Rizzoli, and Bob Weller, for useful discussions and comments. Special thanks are extended to Brad Butman at USGS Woods Hole for making available STRESS subsurface mooring data. Support for preparation of the manuscript at SIO was provided by The Mellon Foundation and by the Minerals Management Service under Cooperative Agreement 14-35-0001-30571.

REFERENCES

Alessi, C. A., S. J. Lentz, and R. C. Beardsley, 1991: The Shelf Mixed Layer Experiment (SMILE): Program overiew and moored and coastal array data report. WHOI Tech. Rep. 91-39, 211 pp. [Woods Hole Oceanographic Institution, Woods Hole, MA 02543-1541.]

Allen, J. S., and P. K. Kundu, 1978: On the momentum, vorticity and mass balance on the Oregon shelf. *J. Phys. Oceanogr.,* **8,** 13–27.

Badan-Dangon, A., K. H. Brink, and R. L. Smith, 1986: On the dynamical structure of the mid-shelf water column off northwest Africa. *Contin. Shelf Res.,* **5,** 629–644.

Barth, J. A., 1994: Short-wavelength instabilities on coastal jets and fronts. *J. Geophys. Res.,* **99,** 16 095–16 115.

Beardsley, R. C., and S. J. Lentz, 1987: The Coastal Ocean Dynamics Experiment collection: An introduction. *J. Geophys. Res.,* **92,** 1455–1464.

Brink, K. H., J. H. LaCasce, and J. D. Irish, 1994: The effect of short-scale wind variations on shelf currents. *J. Geophys. Res.,* **99,** 3305–3314.

Brown, W. S., J. D. Irish, and C. D. Winant, 1987: A description of subtidal pressure field observations on the northern California continental shelf during the Coastal Ocean Dynamics Experiment. *J. Geophys. Res.,* **92,** 1605–1635.

Bryden, H. L., D. Halpern, and R. D. Pillsbury, 1980: Importance of eddy heat flux in a heat budget for Oregon coastal waters. *J. Geophys. Res.,* **85,** 6649–6653.

Chapman, D. C., 1987: Application of wind-forced, long, coastal-trapped wave theory along the California coast. *J. Geophys. Res.,* **92,** 1798–1816.

Chen, D., 1990: Dynamics of time-variable coastal upwelling. Ph.D. thesis, State University of New York at Stony Brook, 83 pp.

——, and D.-P. Wang, 1990: Simulating the time-variable coastal upwelling during CODE-2. *J. Mar. Res.,* **48,** 335–338.

Csanady, G. T., 1982: *Circulation in the Coastal Ocean.* D. Reidel, 279 pp.

Davis, R. E., and P. S. Bogden, 1989: Variability on the California shelf forced by local and remote winds during the coastal ocean dynamics experiment. *J. Geophys. Res.,* **94,** 4673–4783.

de Szoeke, R. A., and J. G. Richman, 1984: On wind-driven mixed layers with strong horizontal gradients—A theory with application to coastal upwelling. *J. Phys. Oceanogr.,* **14,** 364–377.

Dever, E. P., 1995: Subtidal cross-shelf circulation on the northern California shelf. Ph.D. thesis, Massachusetts Institute of Technology/Woods Hole Oceanographic Institution. [Woods Hole Oceanographic Institution, Woods Hole, MA 02543-1541.]

——, and S. J. Lentz, 1994: Heat and salt balances over the northern California shelf in winter and spring. *J. Geophys. Res.,* **99,** 16 001–16 017.

Dickey, T. D., and J. C. Van Leer, 1984: Observations and simulation of a bottom Ekman layer on a continental shelf. *J. Geophys. Res.,* **89,** 1983–1988.

Draper, N. R., and H. Smith, 1966: *Applied Regression Analysis.* John Wiley & Sons, 407 pp.

Fredericks, J. J., J. H. Trowbridge, A. J. Williams III, S. J. Lentz, B. Butman, and T. F. Gross, 1993: Fluid mechanical measurements within the bottom boundary layer over the northern California continental shelf during STRESS. WHOI Tech. Rep. 93-32, 116 pp. [Woods Hole Oceanographic Institute, Woods Hole, MA 02543-1541.]

Grant, W. D., A. J. Williams, and S. M. Glenn, 1984: Bottom stress estimates and their prediction on the northern California continental shelf during CODE-1: The importance of wave-current interaction. *J. Phys. Oceanogr.,* **14,** 506–527.

Gross, T. F., A. E. Isley, and C. R. Sherwood, 1992: Estimation of stress and bed roughness during storms on the northern California shelf. *Contin. Shelf Res.,* **12,** 389–413.

Halpern, D., R. L. Smith, and E. Mittelstaedt, 1977: Cross-shelf circulation on the continental shelf off northwest Africa during upwelling. *J. Mar. Res.,* **35,** 787–796.

Hickey, B. M., and N. E. Pola, 1983: The seasonal alongshore pressure gradient on the west coast of the United States. *J. Geophys. Res.,* **88,** 7623–7633.

Janowitz, G. S., and L. J. Pietrafesa, 1980: A model and observations of time-dependent upwelling over the mid-shelf and slope. *J. Phys. Oceanogr.,* **10,** 1574–1583.

Jenter, H. L., and O. S. Madsen, 1989: Bottom stress in wind-driven depth-averaged coastal flows. *J. Phys. Oceanogr.,* **19,** 962–974.

Kosro, P. M., A. Huyer, S. R. Ramp, R. L. Smith, F. P. Chavez, T. J. Cowles, M. R. Abbott, P. T. Strub, R. T. Barber, P. Jessen, and L. F. Small, 1991: The structure of the transition zone between coastal waters and the open ocean off northern California, winter and spring 1987. *J. Geophys. Res.,* **96,** 14 707–14 730.

Kundu, P. K., 1976: Ekman veering observed near the ocean bottom. *J. Phys. Oceanogr.,* **6,** 238–242.

——, and J. S. Allen, 1976: Some three-dimensional characteristics

of low-frequency current fluctuations near the Oregon coast. *J. Phys. Oceanogr.*, **6,** 181–199.

——, and R. C. Beardsley, 1991: Evidence of a critical Richardson number in moored measurements during the upwelling season off northern California. *J. Geophys. Res.*, **96,** 4855–4868.

Large, W. G., and S. Pond, 1981: Open ocean momentum flux measurements in moderate to strong winds. *J. Phys. Oceanogr.*, **11,** 324–336.

Lentz, S. J., 1987a: A heat budget for the northern California shelf during CODE 2. *J. Geophys. Res.*, **92,** 14 491–14 509.

——, 1987b: A description of the 1981 and 1982 spring transitions over the northern California shelf. *J. Geophys. Res.*, **92,** 1545–1567.

——, 1992: The surface boundary layer in coastal upwelling regions. *J. Phys. Oceanogr.*, **22,** 1517–1539.

——, and J. H. Trowbridge, 1991: The bottom boundary layer over the northern California shelf. *J. Phys. Oceanogr.*, **21,** 1186–1201.

Limeburner, R., Ed., 1985: CODE-2: Moored array and large-scale data report. WHOI Tech. Rep. 85-35, 234 pp. [Available from Woods Hole Oceanographic Institution, Woods Hole, MA 02543-1541.]

López, M., and A. J. Clarke, 1989: The wind-driven shelf and slope water flow in terms of a local and remote response. *J. Phys. Oceanogr.*, **19,** 1092–1101.

Pedlosky, J., 1979: *Geophysical Fluid Dynamics.* Springer-Verlag, 624 pp.

Richman, J. G., and A. Badan-Dangon, 1983: Mean heat and momentum budgets during upwelling for the coastal waters off northwest Africa. *J. Geophys. Res.*, **88,** 2626–2632.

Rudnick, D. L., and R. E. Davis, 1988: Mass and heat budgets on the northern California shelf. *J. Geophys. Res.*, **93,** 14 013–14 024.

Send, U., R. C. Beardsley, and C. D. Winant, 1987: Relaxation from upwelling in the coastal ocean dynamics experiment. *J. Geophys. Res.*, **92,** 1683–1698.

Smith, R. L., 1981: A comparison of the structure and variability of the flow field in three coastal upwelling regions: Oregon, northwest Africa, and Peru. *Coastal Upwelling,* F. A. Richards, Ed., Amer. Geophys. Union, 107–118.

Trowbridge, J. H., and S. J. Lentz, 1991: Asymmetric behavior of an oceanic boundary layer above a sloping bottom. *J. Phys. Oceanogr.*, **21,** 1171–1185.

Weatherly, G. L., and P. J. Martin, 1978: On the structure and dynamics of the oceanic bottom boundary layer. *J. Phys. Oceanogr.*, **8,** 557–570.

Winant, C. D., R. C. Beardsley, and R. E. Davis, 1987: Moored wind, temperature, and current observations made during coastal ocean dynamics experiments 1 and 2 over the northern California shelf and upper slope. *J. Geophys. Res.*, **92,** 1569–1604.

Zamudio, L., and M. López, 1994: On the effect of the alongshore pressure gradient on numerical simulations over the northern California shelf. *J. Geophys. Res.*, **99,** 16 117–16 129.